Hindawi
Journal of Spectroscopy
Volume 2020, Article ID 9067684, 11 pages
https://doi.org/10.1155/2020/9067684

Research Article

Pore Structure Petrophysical Characterization of the Upper Cretaceous Oil Shale from the Songliao Basin (NE China) Using Low-Field NMR

Xin Liu,[1,2] Jinyou Zhang,[1] Yunfeng Bai,[1] Yupeng Zhang,[1] Ying Zhao,[1] Xinyang Cheng,[1] Jiancai Lv,[1] Hui Yang,[1] and Jun Liu [3,4]

[1]*Exploration and Development Research Institute of Daqing Oilfield Co Ltd., Daqing 163712, China*
[2]*Heilongjiang Key Laboratory of Tight Oil and Shale Oil Accumulating Research, Daqing 163712, China*
[3]*Institute of New Energy and Low-Carbon Technology, Sichuan University, Chengdu 610065, China*
[4]*Beijing Key Laboratory of Unconventional Natural Gas Geological Evaluation and Development Engineering, China University of Geosciences, Beijing 100083, China*

Correspondence should be addressed to Jun Liu; j.liu@scu.edu.cn

Received 5 November 2019; Revised 25 December 2019; Accepted 14 January 2020; Published 10 February 2020

Academic Editor: Jose M. Pedrosa

Low-field NMR theory was employed to study the pore structure of the upper cretaceous oil shale, on the basis of fourteen core samples collected from Qingshankou (UCQ) and Nenjiang (UCN) formations in the Songliao basin. Results indicated that the T_2 spectra from NMR measurements for collected samples contain a dominant peak at $T_2 = 1\sim10$ ms and are able to be categorized as three types—unimodal, bimodal, and trimodal distributions. The various morphologies of T_2 spectra indicate the different pore type and variable connection relationship among pores in shale. By contrast, UCN shale has more single pore type and adsorption pores than UCQ shale. Besides, NMR-based measurements provide reliable characterization on shale porosity, which is verified by the gravimetric approach. Porosities in both UCN and UCQ shales have a wide range (2.3%~12.5%) and suggest the strong heterogeneity, which partly makes the challenge in selection of the favorable area for shale oil exploration in the Songliao basin. In addition, the pore size of the collected sample has two distribution types, namely, peaked at ~10 nm and peaked at ~100 nm. Similarly, two distribution patterns emerge to the specific surface area of the study shale—peaked at ~2 nm^{-1} and peaked at ~20 nm^{-1}. Here, more investigations are needed to clarify this polarization phenomenon. Basically, this study not only exhibits a preliminary understanding on the pore structure of the upper cretaceous oil shale, but also shows the reliability and pertinency of the low-field NMR technique in the petrophysical characterization of the shale oil reservoir. It is expected that this work is helpful to guide the investigation on the pore structure of oil shale from the Songliao basin in theory.

1. Introduction

Against this background of growing energy demand to support the betterment of mankind, shale oil is treated as a remarkable supplement and plays an increasingly important role in the world's energy portfolio [1–4]. Following the successful oil extraction from shale in North America, China recently started to explore shale oil resources. Chinese oil shale resources are widely distributed and occur in 47 basins, among which the Songliao basin (NE China) is one of the most important and largest oil fields [5, 6]. Furthermore, the shales from Upper Cretaceous Qingshankou (UCQ) and Nenjiang (UCN) formations in the Songliao basin are organic-rich and thus have an excellent hydrocarbon potential for shale oil exploration [7, 8].

According to the U.S. Geological Survey Estimation, the average technically recoverable oil shale resources from UCQ and UCN formations in the Songliao basin stands at 3.3 billion barrels [9], allowing these two formations to be hotspots for shale oil development in China and to attract extensive attention in the recent years. Geochemical analyses suggested that UCQ and UCN formations were deposited in

a eutrophic and alkaline palaeolake with high salinity and anoxic bottom water conditions during organic matter accumulation [6, 10]. Jia et al. [10] also stated that clay minerals, microbial activity, and detrital matter input have notable influences on the enrichment of organic matter in the UCQ and UCN formations. Sequence stratigraphy and geochemistry indicated the UCQ formation has a better hydrocarbon source rock potential and slightly higher oil yield during pyrolysis than UCN formation [11]. For UCQ formation, its clay content averages 55% [12], raising concerns that it might not be amenable to effective hydraulic fracturing. Although UCQ and UCN shales are mentioned a lot, the characterization of their pore structure is rarely presented in recent research.

Pore space determines the storage capacity for shale oil in the free phase, while the connectivity between pores controls the fluid flow in shale [13–15]. These make the advanced characterization on the pore structure be necessary for better development of shale oil with regards to UCQ and UCN formations. Many approaches are capable of characterizing the shale pore structure, including scanning electron magnetic (SEM), helium porosimetry (HP), and transmission electron microscopy (TEM) [16]. Due to the ultrafine grained microfabric and microlevel heterogeneity of shale, the conventional methods above are defective and unable to examine the entire pore network [16]. In order to remedy this defect, low-field NMR technique, as a time-consuming, convenient, and nondestructive method, gradually enters the mainstream for measuring the pore structure by quantifying the interactions of protons and the porous media [17, 18]. In this study, low-field NMR methodology is introduced to describe the pore structure of the UCQ and UCN shales, which is beneficial for the shale oil industry in the Songliao basin, especially for the resource estimation and reservoir evaluation. In addition, the approaches of mercury injection porosimetry (MIP) and low-temperature N_2 adsorption/desorption (LTNA) are also employed to verify the accuracy of the NMR-based strategy.

2. Geological Background

As the largest continental sedimentary basin in northeastern China, the Songliao basin is a typical Mesozoic basin superimposed on the Palaeozoic basement [11]. The basin evolution can be subdivided into prerift doming, synrift subsidence, postrift thermal subsidence, and structural inversion stages. Referring to the caprock features, the Songliao basin includes six first-order structural units (Figure 1): Northeastern Uplift Zone, Western Slope Zone, Central Depression Zone, Northern Plunge Zone, Southeastern Uplift Zone, and Southwestern Uplift Zone [6, 10].

The thickness of the Cretaceous strata in this continental retroarc basin reaches up to 7000 m, where the UCQ and UCN formations are mainly distributed at the Central Depression Zone and were deposited during the postrift phase characterized by strong subsidence [11, 19, 20]. The sedimentary of UCQ formation occurred from 92.0 to 86.2 Ma. The organic-rich member (lowest of UCQ formation) is 60–135 m thick, covering an area of 87 km^2. The UCN formation was deposited from 84.5 to 79.1 Ma [19, 20]. The oil shale (first and second members) of UCN formation has a composite thickness of 200–400 m and covers an area smaller than that of the UCQ formation (Figure 1) [19]. The UCQ formation has a maximum depth of about 2500 m, while the UCN formation is 0–1900 m deep [21, 22]. The UCQ and UCN formations both contain Type I kerogen and are mainly within the oil window with vitrinite reflectance (R_o) values in the basin center exceeding 1.1%, decreasing below 0.5% near the basin margins [12, 19]. As a result, in the Songliao basin, UCQ and UCN formations are the vital source rocks for conventional petroleum development, as well as the primary target for shale oil exploration.

3. Materials and Analytical Methods

3.1. Samples. A total of fourteen oil shale core samples were collected for this study, among which seven samples were from UCQ formation and the rest came from UCN formation (Table 1). The sampling wells are located on the Central Depression Zone of the middle-north Songliao basin (Figure 1). By X-ray diffraction analysis, minerals in both UCQ and UCN shale samples were found to be mainly quartz and clay minerals, with a supplement of feldspar, carbonate minerals, and pyrite. Compared with the UCQ shale, the UCN shale sample had higher quartz content and lower content of clay minerals, on average (Figure 2). For the UCQ shale, the R_o varies from 0.75% to 1.30% and averages 0.99%, and the total organic carbon (TOC) is in the range 0.71%~5.43% with a mean of 2.33% (Table 1). As far as the UCN shale, the R_o values have a distribution of 0.60%~0.75% (average of 0.67%), and the TOC averages 1.36% with a range of 0.79%~3.78% (Table 1).

3.2. Low-Field NMR Measurement

3.2.1. Basic Principle of Low-Field NMR. Generally, NMR signals are usually motivated by the activity of magnetic nuclei (e.g., hydrogen proton) in the magnetic field [23, 24]. In this study, the NMR measurements were performed using an analyzer of the MicroMR12-025V type (Shanghai Niumag Corporation, PRC) with a magnetic strength of 0.28 T using a 25.4 mm diameter magnet coil which generates a homogeneous and stable field gradient. The low magnetic field with a frequency of 11.792 MHz makes the NMR signal come from the ^{1}H-fluid in the pore rather than from the solid skeleton of the oil shale [25, 26].

By using low-field NMR, the number of hydrogen atoms present in the CH_4 molecule can be detected through the measurement of transverse relaxation times (T_2) [27]. In general, a typical T_2 expression keeps connection with the surface relaxation related to the pore structure, the bulk relaxation of fluid precession, and the diffusion relaxation resulted from the gradient field [28, 29]. Accordingly, in a porous media, the compete T_2 relaxation submits to the following equation:

$$\frac{1}{T_2} = \frac{1}{T_{2B}} + \frac{1}{T_{2S}} + \frac{1}{T_{2D}}, \quad (1)$$

where the subscripts B, S, and D represent the bulk, surface, and diffuse relaxations, respectively. Among the above

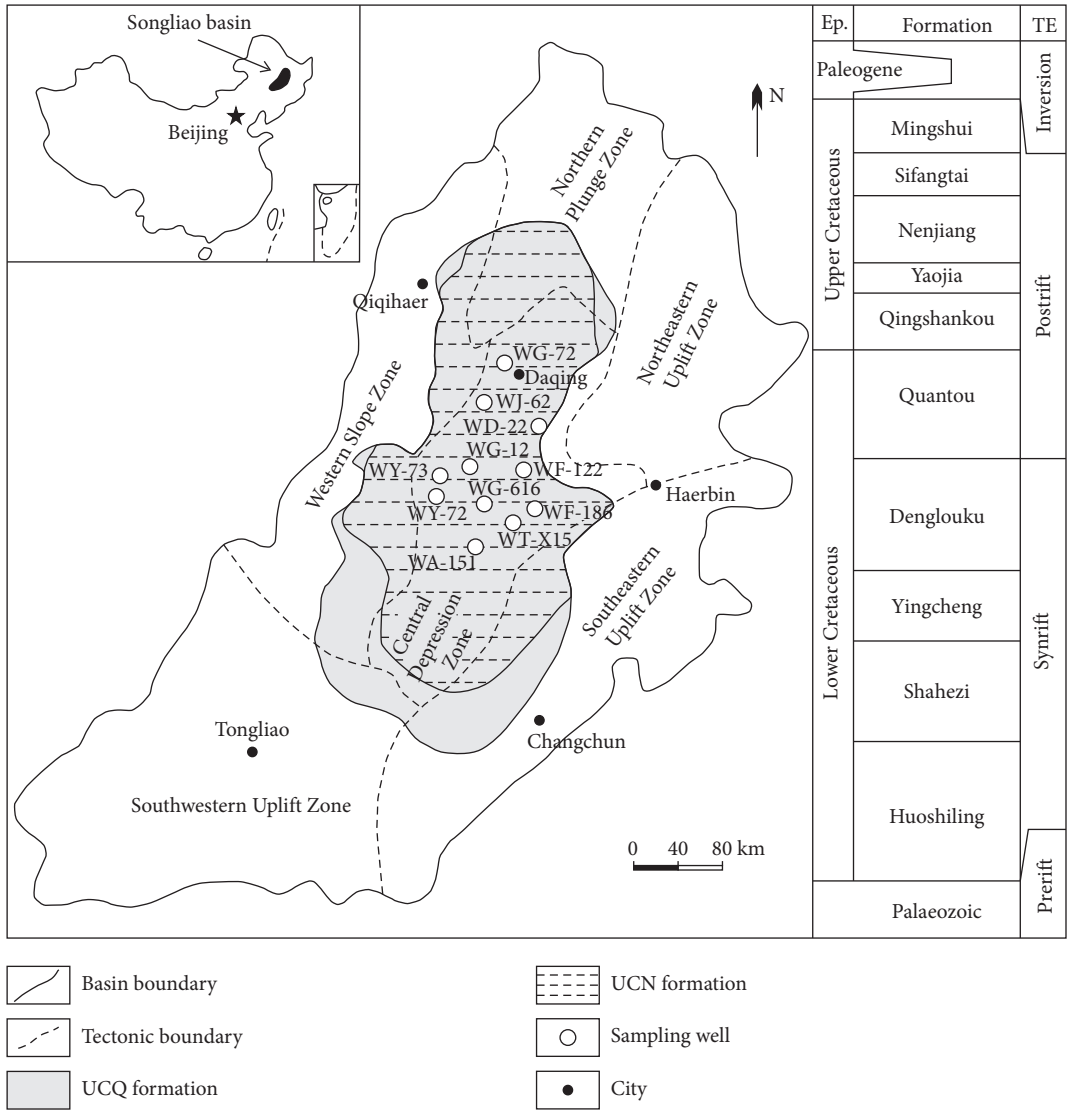

Figure 1: Sketch map of structural units and stratigraphic column of the Songliao basin with the location of sampling well (modified from Jia et al. [10] and Xu et al. [11]). Ep: epoch; TE: tectonic evolution.

Table 1: Basic information of collected oil shale samples.

Upper Cretaceous Qingshankou (UCQ) formation					Upper Cretaceous Nenjiang (UCN) formation				
Sample ID	Sampling well	Depth (m)	TOC (%)	R_o (%)	Sample ID	Sampling well	Depth (m)	TOC (%)	R_o (%)
F34	WF-122	1629.0	5.43	0.75	Y39	WY-72	1437.3	0.87	0.65
D05	WD-22	1921.3	1.67	0.80	Y40	WY-72	1438.0	0.79	0.65
T49	WT-X15	1943.1	2.15	0.80	F63	WF-186	984.2	0.94	0.60
Y38	WY-73	2325.8	2.07	1.30	J100	WJ-62	1667.0	1.13	0.75
G57	WG-616	1875.6	0.71	1.10	G80	WG-12	1390.3	0.97	0.60
G24	WG-72	2110.8	2.29	1.10	G82	WG-12	1705.7	3.78	0.70
A16	WA-151	2080.5	2.01	1.10	G77	WG-22	1521.0	1.07	0.75

TOC, total organic carbon; R_o, vitrinite reflectance. Locations of sampling wells are shown in Figure 1.

parameters, the diffuse relaxation is generated in a magnetic field gradient. Therefore, the homogeneous and stable field gradient enables the ratio $1/T_{2D}$ to be small enough to be ignored. Bulk relaxation of a pure liquid fluid is an intrinsic property and relaxes slowly with a usual time of 2–3 s, making $T_{2B} \gg T_2$ and thus the ratio $1/T_{2B}$ will also be negligibly small in equation (2) [30]. Consequently, the subsistent T_2 relaxation in this study yields [31, 32]

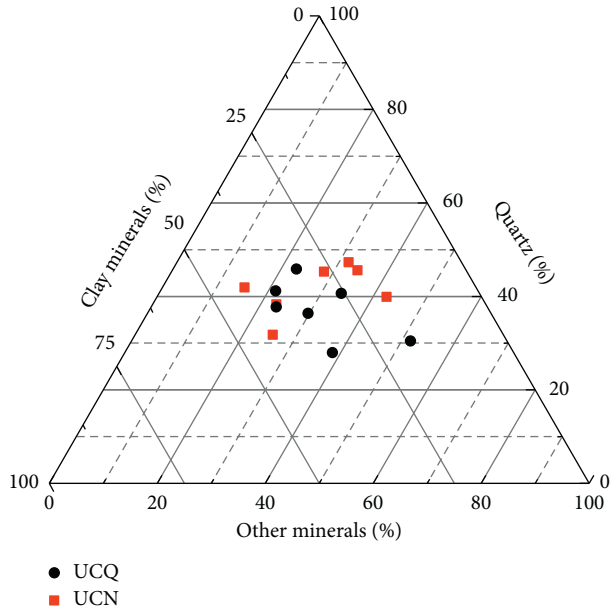

Figure 2: Mineral composition of collected samples. UCQ, Upper Cretaceous Qingshankou formation; UCN, Upper Cretaceous Qingshankou Nenjiang formation.

$$\frac{1}{T_2} \approx \frac{1}{T_{2S}} = \rho_2\left(\frac{S}{V}\right), \tag{2}$$

where ρ_2 is the surface relaxivity with a constant value of about 0.05 μm/ms for shale based on the work of Sondergeld et al. [33] and S/V is the surface-to-volume ratio (namely, specific surface area). For simplification purpose, the pore geometry of shale is regarded as a cylinder, so S/V equals $2/r$ [34]. In this situation, equation (2) can be transformed into

$$r = 100 \times T_2, \tag{3}$$

where r is the shale pore radius (nm) and the conversion parameter (100) has a unit of nm/ms.

Equations (2) and (3) indicating a faster T_2 relaxation correspond with a smaller pore size, and vice versa. During the NMR experiments, the main setting parameters, including waiting time of 3500 ms, echo interval of 0.12 ms, echo number of 10000, and scan times of 64, were adopted to enable the measurements to capture the maximum recovery of the polarized NMR T_2 signal and the fast relaxation components.

3.2.2. Experimental Operations. All oil shale samples were cut into core plugs with a diameter of 2.5 cm and a length of 5 cm. Each sample was detected twice by the NMR instrument under two different pretreatments—hydrocarbon/water removal (Step I) and hydrocarbon saturated (Step II). The difference between two measurements is adopted to expose the hydrocarbon information in shale pores, enabling the investigation on the pore morphology, porosity, pore size distribution (PSD), and specific surface area.

Step I. Hydrocarbon/water removal: the NMR T_2 signal from residual ^{1}H-fluid in completely closed pores of the shale.

Firstly, collected samples were placed in an oil-cleaned instrument after being wrapped with the filter paper, under a constant temperature of 90°C (363.15 K). Secondly, hydrocarbon and water in connected pores were extracted by circulating the dichloromethane and acetone vapor for 72 h. Then, the treated samples were placed in an NMR detector to record their T_2 spectra at 35°C (308.15 K).

The T_2 measurements were used to explore the information of closed pores in the shale with the assumption that the completely closed pores are 100% filled by the same ^{1}H-fluid for all samples.

Step II. Hydrocarbon saturated: the NMR T_2 signal from the saturated solution in an effective pore volume of shale.

Firstly, after hydrocarbon/water removal, all shale samples were vacuumed in a vacuum oven for 24 h and then fully saturated with n-dodecane (n-C_{12}) for 48 h under a pressure of 10 MPa. Secondly, these n-C_{12}-saturated shale plugs were wrapped with a nonmagnetic film to prevent the evaporation of n-C_{12}. Then, n-C_{12}-saturated samples were conducted by NMR measurements at 35°C (308.15 K).

Subsequently, the T_2 signals from n-C_{12}-saturated plugs (Step II) minus those from hydrocarbon/water removed plugs (Step I) are supposed to be the T_2 signals of n-C_{12} in the effective pore volume of shale. Accordingly, by employing n-C_{12} as a probe, these NMR measurements are the basis in this study to enhance the knowledge of connected pores in the shale.

3.3. Accuracy Validation of NMR Measurement. Currently, there is no universal operation standard for the NMR methodology, in spite that it is described as a sophisticated approach. Thus, the accuracy of NMR measurements needs to be validated to enhance its reliability. In this study, the pore structure derived from the NMR approach was verified by LTNA and MIP operations which have sophisticated and universal operation standard. The LTNA and MIP methods have different strengths and weaknesses [35], thus their combination is more reliable in the accuracy validation of the NMR measurement.

LTNA experiments were performed for all collected samples by using a BSD-PS Type surface area and porosity analyzer, following the standard of SY/T 6154-1995 (that is, characterization on specific surface and pore size distribution of rock from N_2 adsorption). For sample preparation, the oil shale samples were grinded and sieved to 60–80 mesh. Then, the powders were dried at 150°C (423.15 K) for 3 h in a vacuum oven. During LTNA measurements, the N_2 adsorption isotherms were obtained from recording adsorption and desorption volumes at −196°C (77.15 K) with the relative pressure (P/P_0) ranging from 0.01 to 0.995.

Complying with the standard of GB/T21650.1–2008 (namely, pore size distribution and porosity of solid materials by mercury porosimetry and gas adsorption–Part 1: mercury porosimetry), MIP measurements for all collected samples were conducted by a GT60 Type instrument which has a capacity to recognize pore sizes of 0.0036~950 μm. Before MIP tests, oil shale samples were crushed and sieved

into fine fragments with a diameter of 2~3 mm. The fragments were transferred into a dilatometer (volume of 1 cm^3) after being dried at 110°C (383.15 K). Followed by vacuuming the dilatometer, the intrusion and extrusion curves were obtained from recording the injected and ejected volumes of mercury. In this study, the maximum pressure of mercury injection reaches to as high as 200 MPa (i.e., ~29000 psi). The relationship between pore size and MIP pressure is reported by Fangwen et al. [35] and Seiphoori et al. [36].

4. Results and Discussion

According to the series of experiments, this section will discuss how NMR relaxation (T_2 spectra) can be used as an independent tool for classifying the shale pore types and morphology, calculating porosity, and evaluating pore size distribution (PSD) and specific surface area. Considering that the petrophysical properties are of significance for shale oil exploration and exploitation, this section is supposed to be a great theoretical implication for the shale oil industry in UCQ and UCN shale formations of Songliao basin, NE China. Note that this section works with the precondition that the in-site oil (in fact, multifluid mixtures) is simulated by pure n-C_{12}, and with the overlook of the extremely small pores cannot be filled by n-C_{12}.

4.1. NMR T_2 Spectra. The NMR T_2 spectra from a sample with different pretreatments have obviously variable characteristics. Under the circumstance of hydrocarbon/water removal, NMR T_2 spectra exhibit small amplitude and thus indicate that the residual ^{1}H-fluid in completely closed pores of shale is scarce (Figure 3). Comparatively, distinct amplitude emerges to the samples saturated with n-C_{12}, suggesting that considerable amount of n-C_{12} is injected into effective pores in the oil shale to enable the T_2 amplitude to be raised significantly (Figure 3). By subtraction processing, the T_2 spectra motivated by the n-C_{12} in effective pores are plotted (Figures 3 and 4), which is actually adopted for the investigation on the pore structure of the collected oil shale samples in this work.

It is intuitively plausible that three kinds of T_2 spectra are obtained by NMR experiments: unimodal distribution (e.g., sample D05), bimodal distribution (e.g., sample Y40), and trimodal distribution (e.g., sample F34) (Figures 3 and 4). For all samples, the NMR spectra have a dominant peak at a T_2 value of about 1~10 ms. Basically, the measured NMR spectra exhibit a diversity morphology and a wide T_2 value of the dominant peak, which notes that the pore structure of the Upper Cretaceous oil shale is complicated. This is because that the T_2 spectra with diverse characteristics usually represent different pore structures.

Furthermore, the characteristic of NMR T_2 spectra for the UCQ shale differs from that for the UCN shale. For example, more unimodal T_2 spectra emerge to the UCN shale rather than the UCQ shale, according to the NMR measurements (Figures 3 and 4). This phenomenon intuitively reveals the difference of pore structure in UCQ and UCN shale samples, further enabling the significance of petrophysical characterization in this study.

4.2. Pore Type and Morphology. Because of the sedimentary, diagenesis, and tectonism, shale is usually characterized as strong heterogeneity and thus contains various pore types [37, 38]. As verified by Yao et al. [25], NMR T_2 amplitude is able to indicate the pore type and morphology. In this study, The NMR T_2 distributions are commonly unimodal and bimodal and sometimes trimodal (Figures 3 and 4). Referring to the criterion created by Yao et al. [25], a narrow unimodal T_2 distribution represents a single pore type (e.g., samples G80 and F63), whereas a wide one suggests multiple pore types (e.g., sample G57) (Figure 4). For multiple NMR T_2 peaks (bimodal and trimodal), the connection among these peaks can be used to identify the connectivity among pores [25]. For example, the well-connected bimodal/trimodal T_2 distributions (e.g., samples G24 and G82) suggest that well-connective multipores exist in these oil shale samples (Figure 4). By contrast, the less well-connected bimodal/trimodal T_2 distributions (e.g., samples Y39 and T49) may indicate that pores in different size are disconnected in these samples. In addition, as per the achievements by Li et al. [34], adsorption pores commonly exist in the samples with unimodal, bimodal, or trimodal T_2 distributions, while seepage pores are mainly developed in the samples with bimodal or trimodal T_2 distributions.

Both UCQ and UCN shale samples had pores poorly connected because well-connected bimodal/trimodal T_2 spectra are less frequent in study samples (Figure 4). Nevertheless, UCQ and UCN shale samples, by contrast, have some different pore types, on the basis of the NMR T_2 spectra. It seems that the sample with a single pore type and adsorption pore is more common for the UCN shale since there are more unimodal T_2 spectra with narrow distribution (Figure 4).

Furthermore, LTNA is employed to analyze the correctness of NMR T_2 distribution in describing the pore type and morphology. According to the International Union of Pure and Applied Chemistry (IUPAC) classification, the N_2 adsorption/desorption curve would be described as the Type IV isotherm when a noticeable hysteresis loop exists, which is associated with the limiting uptake over a range of high P/P_o [39]. Accordingly, the N_2 adsorption/desorption curves of the two representative samples are of Type IV (Figure 5). Furthermore, Sing et al. [39] noted that hysteresis appearing in the multilayer range of physisorption isotherms is usually associated with capillary condensation in mesopore structures, where four specific pore structures are identified according to the shape of the hysteresis loops. By this classification, the pore type of sample Y39 belongs to H2 (inkbottle-shaped pore)—a poorly connective pore type, while that of sample G82 primarily is H3 (plate-like pore)—a well-connective pore type (Figure 5). The LTNA results illustrate that the NMR T_2 measurement is reliable in characterizing the pore type of oil shale.

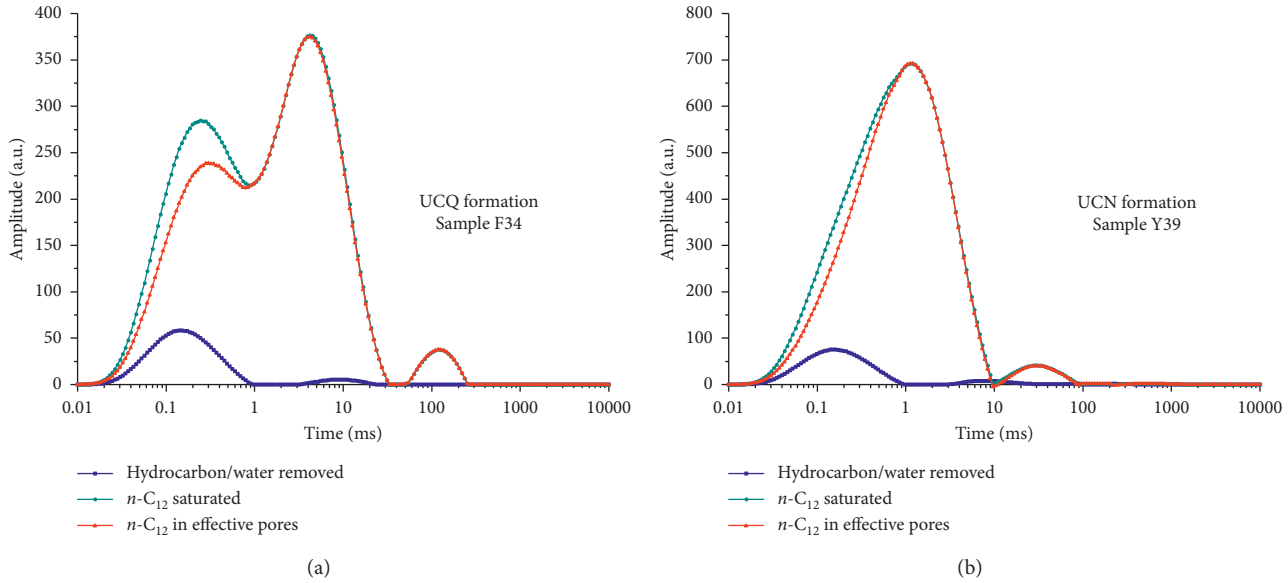

Figure 3: NMR T_2 spectra under different treatments of oil shale. UCQ, Upper Cretaceous Qingshankou (a); UCN, Upper Cretaceous Nenjiang (b).

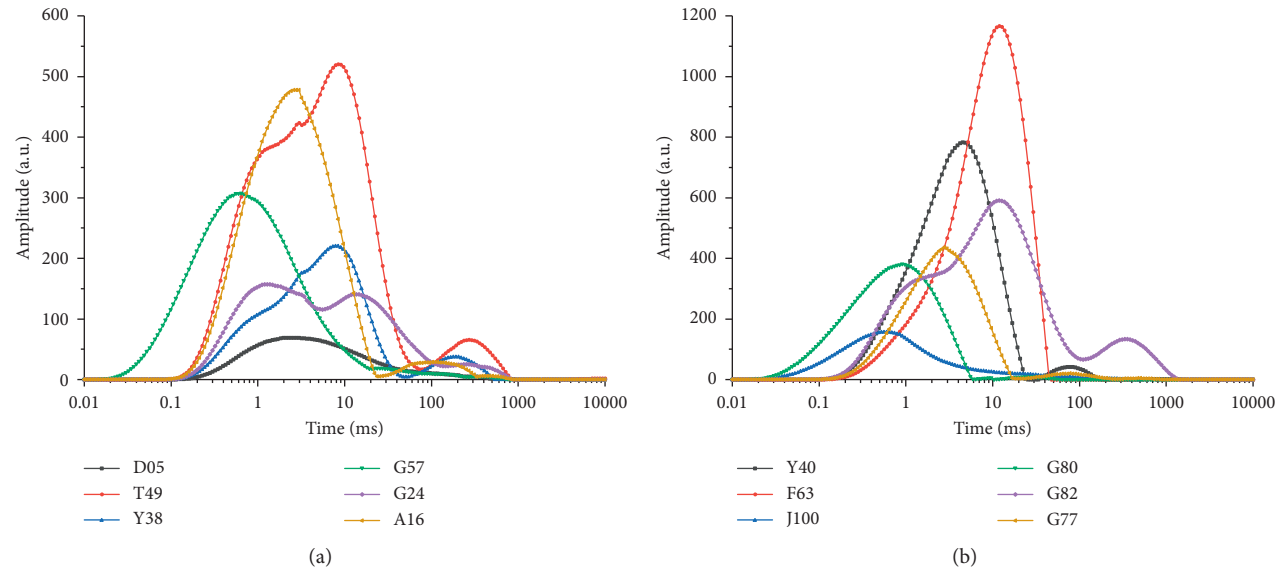

Figure 4: NMR T_2 spectra motivated from n-C_{12} in effective pores of oil shale. UCQ, Upper Cretaceous Qingshankou (a); UCN, Upper Cretaceous Nenjiang (b).

4.3. Effective Porosity. Pores and microfractures provide storage, migration, and seepage channels for oil in shale and thus are of significance for shale oil extraction. Porosity is an extensively used index to evaluate the pore volume of inner pores/fractures in oil shale. Previous studies noted that the signal intensity of the hydrogen-containing fluid (n-C_{12} in this study) in samples is able to investigate the NMR porosity [40–42]. Accordingly, a series of NMR measurements were, respectively, conducted on five standard n-C_{12} samples (0.2, 0.4, 0.6, 0.8, and 1.0 mL). As shown in Figure 6, in this study, there is a clear linear relationship between amplitude and n-C_{12} volume:

$$V_{n\text{-}C_{12}} = 0.3722 \times T_2, \quad (4)$$

where $V_{n\text{-}C_{12}}$ is the n-C_{12} volume (unit: mL) and T_2 is the NMR amplitude motivated by n-C_{12} in pores (10^3 a.u.).

According to the NMR T_2 spectra motivated from n-C_{12} in effective pores (Figures 3 and 4), the effective porosities of collected samples are obtained and plotted in Figure 7, referring to equation (4). In order to clarify the accuracy of NMR-based porosity, gravimetric measurements were employed by weighing the n-C_{12} quality in effective pores of oil shale. The porosity values from NMR and gravimetric approaches present a strong resemblance (Figure 7),

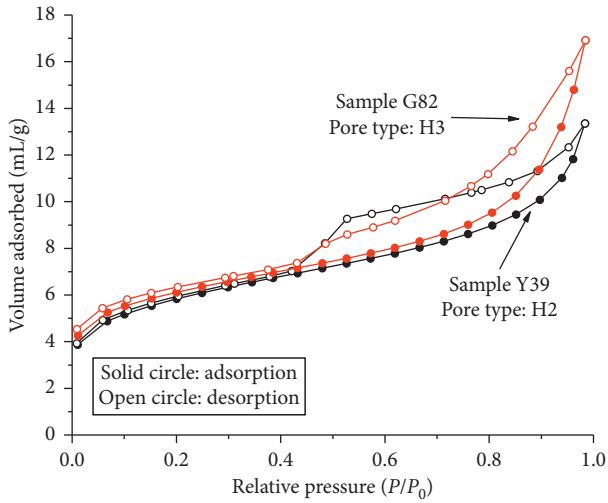

Figure 5: Adsorption/desorption curves of low-temperature (77 K) N_2 analysis.

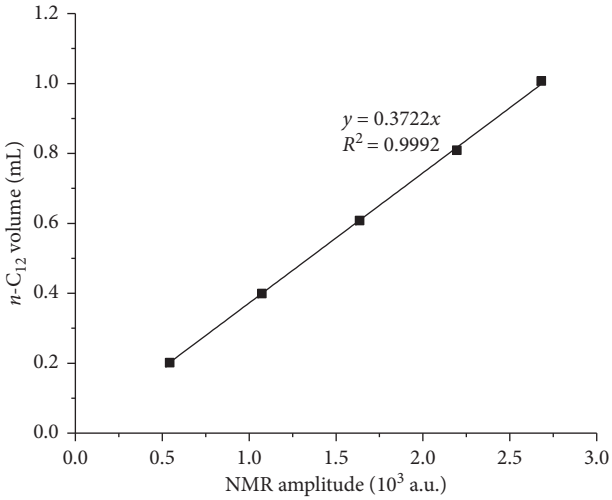

Figure 6: Relationship between NMR amplitude and n-C_{12} volume.

signaling the NMR strategy is reliable in porosity measurement of oil shale. Results exhibit the porosities of collected samples have a range of 2.3%~12.5% with an average of 7.3%, according to the NMR measurements (Figure 7).

The porosity is 7.57% in average for the UCQ shale with a wide range of 2.6%~12.2%, while that averages 6.98% for the UCN shale and varies from 4.5% to 11.6%. The wide range of measured porosity suggests the strong heterogeneity of collected samples, suggesting the nonuniform horizontal distribution of shale oil in UCQ formation or UCN formation. Thus, more attentions should be paid to the selection of area with greater porosity in the future, aiming to guide the shale oil extraction from the UCQ and UCN shale reservoirs.

4.4. Pore Size Distribution. n-C_{12} in different pore sizes shows different relaxation velocities due to the difference of relaxation mechanism and relaxation velocity during NMR

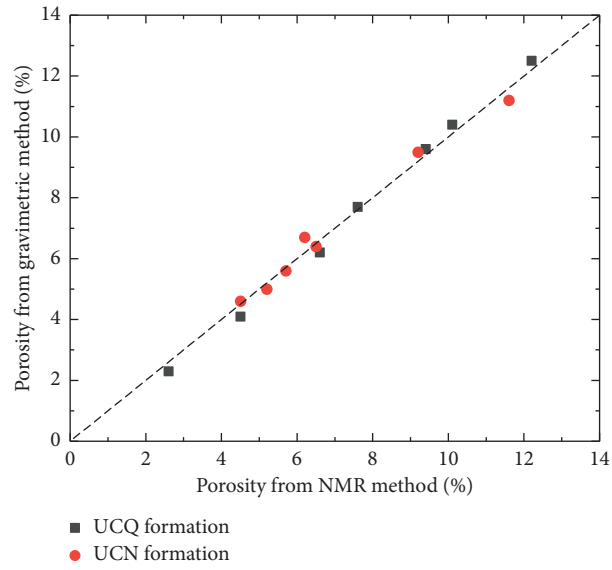

Figure 7: Comparison of porosity values from NMR and gravimetric methods.

measurements. Therefore, the distribution characteristics of the NMR T_2 spectrum have the ability to indirectly reflect the pore size distribution and fluid distribution, according to equation (3): larger pores correspond to longer relaxation time and smaller pores to shorter relaxation time. Taking sample Y40 as a typical example, the PSD derivations from different methods take an attitude that the NMR measurement covers a broader PSD than the LTNA or MIP method (Figure 8). In addition, the NMR-based PSD is regarded as reliable as it is very close to the combined result of LTNA and MIP approaches (Figure 8). Regarding to sample Y40, the pore size varies considerably with a span from 1 nm to 10000 nm, while the pores with diameters of ~100 nm act as the major contributors for total porosity (Figure 8).

Furthermore, the relationships of dV/dD pore volume vs. pore width for all samples are plotted in Figure 9, on the basis of NMR experiments. For both UCQ and UCN formations, there exist two types of PSD curves in Figure 9—peaked at ~10 nm (Type I) and peaked at ~100 nm (Type II). Around 30% of the collected samples hold the Type I PSD curve (Figure 9), where pores with diameters of 1 ~100 nm occupy a dominant proportion among all inner pores of oil shale. PSD curves of major samples (~70%) belong to Type II (Figure 9), with the vast majority of pores being 10~1000 nm in size. Considering the polarization of Type I and Type II, more attentions are expected to be drawn to the mechanism of this phenomenon.

4.5. Specific Surface Area Distribution. Specific surface area (S/V) is a significant parameter in the petrophysical characterization of oil shale. Conventional strategies (like LTNA) provide S/V values but are limited in determining the S/V distribution of a certain shale sample.

According to equation (2), the porous media are generally characterized by the complicated surface structure

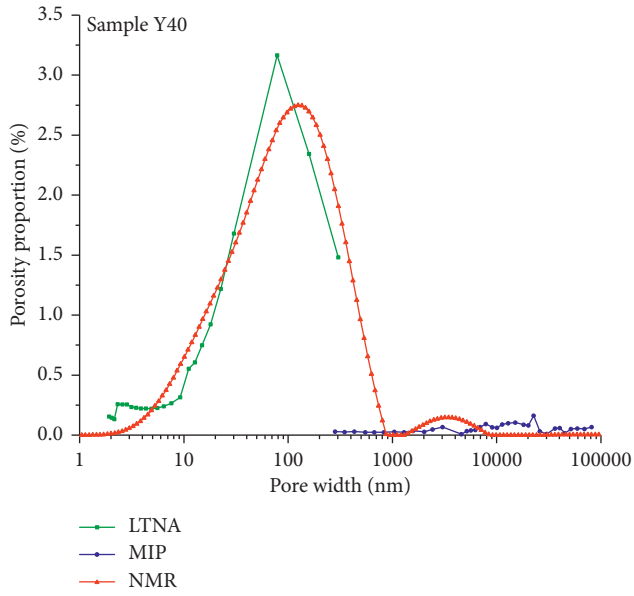

Figure 8: Pore size distribution based on low-temperature N_2 adsorption/desorption (LTNA), mercury injection porosimetry (MIP), and NMR methods.

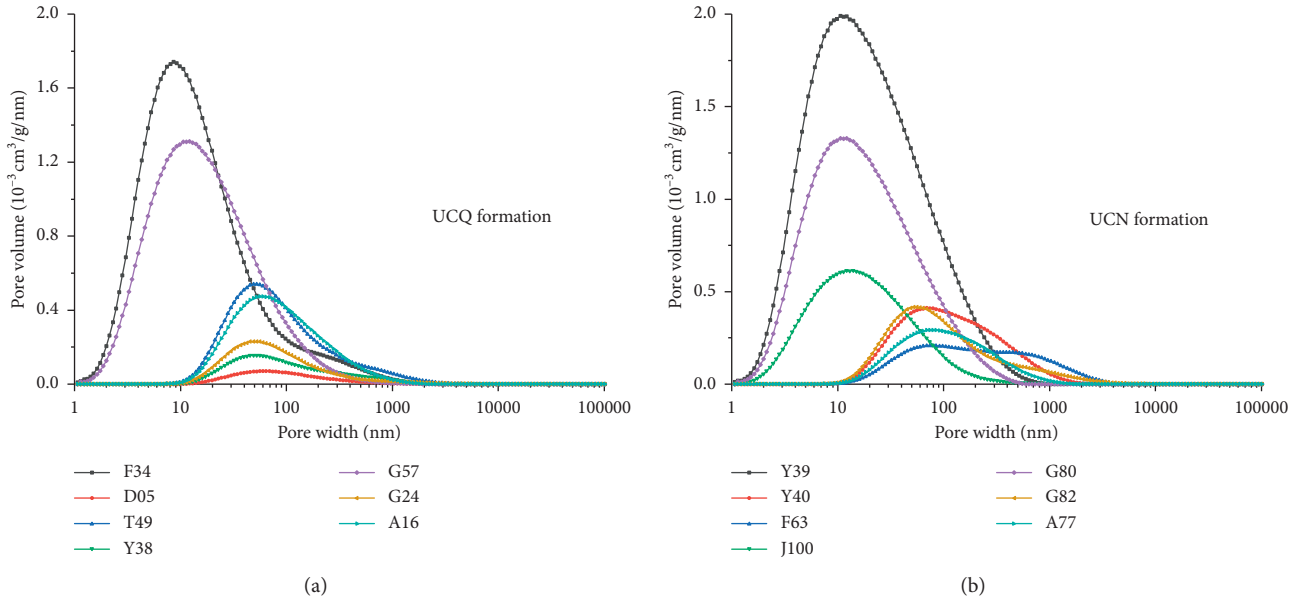

Figure 9: Plots of the pore size distribution (PSD) of collected samples derived from NMR experiments. UCQ formation (a); UCN formation (b).

with strong interaction between pore surface and ^{1}H-fluid (e.g., H_2O and n-C_{12}). Hence, the interaction between n-C_{12} molecules and pore surface can be characterized by T_2 relaxation in this study. Combining equation (2) with equation (3), the S/V of oil shale yields

$$\frac{S}{V} = \frac{1}{T_2 \times \rho_2} = \frac{100}{r \times \rho_2} = \frac{2000}{r}. \quad (5)$$

As per equation (5), the S/V distribution of samples can be obtained. Setting sample Y38 and J100 as representative samples, the S/V distributions are plotted in Figure 10. Basically, shorter T_2 indicates smaller pore size and greater S/V value. On the contrary, the longer the T_2 is, the larger the pores in oil shale and the lower the value of S/V is (Figure 10). Regarding to sample Y38, the S/V ranges from 0.1 nm^{-1} to 200 nm^{-1} and mainly centered at ~2 nm^{-1}. Comparatively, sample J100 has a broader S/V range of 0.08 nm^{-1} ~ 1000 nm^{-1} and mainly peaked at ~20 nm^{-1}. Similar with samples Y38 and J100, the S/V distributions of the rest of the samples are obtained by coordinate transformation of Figures 3 and 4, according to equation (5). This phenomenon indicates that the S/V distribution is able to be clarified as two patterns, that is, peaked at ~2 nm^{-1} (Pattern A) and peaked at ~20 nm^{-1} (Pattern B), based on Figure 9 and equation (5). As for the

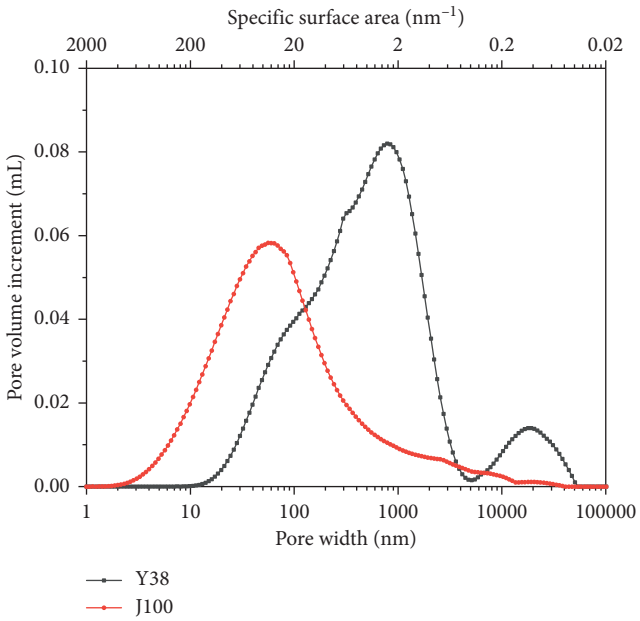

Figure 10: Plots of the specific surface area (S/V) distribution of samples Y38 and J100 based on NMR measurements.

sample with a Pattern A S/V distribution, the S/V is mainly contributed by the pores with a diameter of 10–200 nm. Comparatively, if the S/V distribution is described as Pattern B, the S/V is primarily donated by bigger pores (100–2000 nm).

Basically, in shale samples, pores with smaller S/V benefit to adsorb fluid, while pores with bigger S/V are helpful for the storage-free fluid [38]. Thus, the NMR-based approach for the S/V measurement is conducive to filter the favorable target for shale oil exploration because free oil (rather than adsorbed oil) is potentially the most producible component of tight shale reservoirs [43].

4.6. Outlook of NMR-Based Approach for the Shale Oil Development in Songliao Basin. In this study, the NMR-based methodology exposed a preliminary understanding on the pore structure of oil shale from the Songliao basin, in spite that only fourteen core samples were collected. Compared with the petrophysical characterization using the conventional technique like LTNA, the NMR-based method with the n-C_{12} probe is probably more suitable and reliable to the study on the shale oil reservoir. This is because the N_2 molecule has a smaller diameter than the n-C_{12} molecule and thus tends to probe more pores with extremely small size which cannot store oil. That is to say, the NMR measurement is a more targeted approach to focus on the effective pores for oil storage in shale and thus provide more real scientific investigations.

5. Conclusions

(1) The NMR spectra of all samples have a dominant peak at a T_2 value of about 1~10 ms. The narrow and wide unimodal T_2 distribution represents a single and multiple pore type, respectively. The well-connected bimodal/trimodal T_2 distributions suggest that pores in different size have good connectivity, and vice versa. By contrast, the UCN shale has more single pore type and adsorption pores than the UCQ shale.

(2) As verified by gravimetric measurements, the NMR strategy is reliable in determining the porosity of oil shale. According to the NMR measurements, the porosities of collected samples vary from 2.3% to 12.5% with an average of 7.3%. The wide range of measured porosity suggests that the strong heterogeneity emerges to both UCN and UCQ shale reservoirs from Songliao basin.

(3) As for both UCN and UCQ samples, PSD curves are intuitively clarified as two types—peaked at ~10 nm and peaked at ~100 nm, while S/V distributions are also categorized into two patterns—peaked at ~2 nm^{-1} and peaked at ~20 nm^{-1}. However, more attempts are needed to explain the polarization of PSD and S/V distribution.

Data Availability

The data used to support the findings of this study are available from the corresponding author upon request.

Conflicts of Interest

The authors declare that they have no known competing financial interests or personal relationships that could influence the work reported in this paper.

Acknowledgments

The authors acknowledge financial support from the National Science and Technology Major Projects in the 13th Five Year Plan (2017ZX05001-002), improvement of Fine Oil Exploration Technology and Increase of Scale in Northern Songliao Basin (2016E-0201), and the Beijing Key Laboratory of Unconventional Natural Gas Geological Evaluation and Development Engineering (2019BJ02002).

References

[1] J.-C. Zhang, L.-M. Lin, Y.-X. Li et al., "Classification and evaluation of shale oil," *Earth Science Frontiers*, vol. 19, no. 5, pp. 322–331, 2012.

[2] J. Liu, Y. Yao, Z. Zhu, L. Cheng, and G. Wang, "Experimental investigation of reservoir characteristics of the upper Ordovician Wufeng formation shale in middle-upper Yangtze region, China," *Energy Exploration & Exploitation*, vol. 34, no. 4, pp. 527–542, 2016.

[3] L. Chen, Y.-C. Lu, J.-Y. Wu et al., "Sedimentary facies and depositional model of shallow water delta dominated by fluvial for Chang 8 oil-bearing group of Yanchang formation in southwestern Ordos Basin, China," *Journal of Central South University*, vol. 22, no. 12, pp. 4749–4763, 2015.

[4] T. Saif, Q. Lin, B. Bijeljic, and M. J. Blunt, "Microstructural imaging and characterization of oil shale before and after pyrolysis," *Fuel*, vol. 197, pp. 562–574, 2017.

[5] Z.-J. Liu, Q.-S. Dong, S.-Q. Ye et al., "The situation of oil shale resources in China," *Journal of Jilin University (Earth Science Edition)*, vol. 36, no. 6, pp. 869–876, 2006.

[6] A. Bechtel, J. Jia, S. Strobl et al., "Palaeoenvironmental conditions during deposition of the upper Cretaceous oil shale sequences in the Songliao Basin (NE China): implications from geochemical analysis," *Organic Geochemistry*, vol. 46, pp. 76–95, 2012.

[7] B. Liu, Y.-F. Lü, Q.-C. Ran, C.-L. Dai, M. Li, and M. Wang, "Geological conditions and exploration potential of shale oil in Qingshankou formation, northern Songliao basin," *Oil and Gas Geology*, vol. 35, no. 2, pp. 280–285, 2014.

[8] Y.-L. Zheng, C.-R. Chen, B.-C. Wang, Z.-G. Wang, S.-Y. Liu, and X.-M. Wu, "Resource potential evaluation of oil shale in north Songliao basin," *Journal of Jilin University (Earth Science Edition)*, vol. 45, no. 3, pp. 683–690, 2015.

[9] C. J. Potter, C. J. Schenk, J. K. Pitman et al., *Assessment of Undiscovered Continuous Oil and Gas Resources of Upper Cretaceous Shales in the Songliao Basin of China*, 2018, https://doi.org/10.3133/fs20183014.

[10] J. Jia, A. Bechtel, Z. Liu, S. Strobl, P. Sun, and R. F. Sachsenhofer, "Oil shale formation in the upper Cretaceous Nenjiang formation of the Songliao basin (NE China): implications from organic and inorganic geochemical analyses," *International Journal of Coal Geology*, vol. 113, pp. 11–26, 2013.

[11] J. Xu, Z. Liu, A. Bechtel et al., "Basin evolution and oil shale deposition during upper Cretaceous in the Songliao Basin (NE China): implications from sequence stratigraphy and geochemistry," *International Journal of Coal Geology*, vol. 149, pp. 9–23, 2015.

[12] C. Liu, Z. Wang, Z. Guo et al., "Enrichment and distribution of shale oil in the Cretaceous Qingshankou formation, Songliao basin, northeast China," *Marine and Petroleum Geology*, vol. 86, pp. 751–770, 2017.

[13] X. Han, X. Jiang, L.-J. Yu, and Z. Yu, "Change of pore structure of oil shale particles during combustion. Part 1. Evolution mechanism," *Energy & Fuels*, vol. 20, no. 6, pp. 2408–2412, 2006.

[14] P. Tiwari, M. Deo, C. L. Lin, and J. D. Miller, "Characterization of oil shale pore structure before and after pyrolysis by using X-ray micro CT," *Fuel*, vol. 107, pp. 547–554, 2013.

[15] Y. Gu, W. Ding, M. Yin et al., "Nanoscale pore characteristics and fractal characteristics of organic-rich shale: an example from the lower Cambrian Niutitang formation in the Fenggang block in northern Guizhou Province, South China," *Energy Exploration & Exploitation*, vol. 37, no. 1, pp. 273–295, 2018.

[16] L. N. Listiyowati, "Laboratory characterization of shale pores," *IOP Conference Series: Earth & Environmental Science*, vol. 118, Article ID 012067, 2018.

[17] J. Liu, L. Xie, Y. Yao, Q. Gan, P. Zhao, and L. Du, "Preliminary study of influence factors and estimation model of the enhanced gas recovery stimulated by carbon dioxide utilization in shale," *ACS Sustainable Chemistry & Engineering*, vol. 7, no. 24, pp. 20114–20125, 2019.

[18] Y. Zhao, Y.-F. Sun, S.-M. Liu, K. Wang, and Y.-D. Jiang, "Pore structure characterization of coal by NMR cryoporometry," *Fuel*, vol. 190, pp. 359–369, 2016.

[19] F. Zhi-Qiang, J. Cheng-Zao, X. Xi-Nong, Z. Shun, F. Zi-Hui, and T. A. Cross, "Tectonostratigraphic units and stratigraphic sequences of the nonmarine Songliao basin, northeast China," *Basin Research*, vol. 22, no. 1, pp. 79–95, 2010.

[20] P.-J. Wang, F. Mattern, N. A. Didenko, D.-F. Zhu, B. Singer, and X.-M. Sun, "Tectonics and cycle system of the Cretaceous Songliao basin: an inverted active continental margin basin," *Earth-Science Reviews*, vol. 159, pp. 82–102, 2016.

[21] L. Desheng, "Hydrocarbon habitat in the Songliao rift basin, China," *Geological Society, London, Special Publications*, vol. 80, no. 1, pp. 317–329, 1995.

[22] S.-X. Pan, T.-Q. Wang, P.-S. Wei, J.-G. Wang, C.-Y. Liu, and S.-J. Liang, *Accumulation and Exploration Prospects of Shale Oil and Gas in Songliao Basin, Eastern China*, American Association of Petroleum Geologists, Tulsa, OH, USA, 2010, http://www.searchanddiscovery.com/documents/2010/10272pan/.

[23] K. K. Darrow, "Magnetic resonance," *Bell System Technical Journal*, vol. 32, no. 1, pp. 74–99, 1953.

[24] C. F. Hazlewood, D. C. Chang, B. L. Nichols, and D. E. Woessner, "Nuclear magnetic resonance transverse relaxation times of water protons in skeletal muscle," *Biophysical Journal*, vol. 14, no. 8, pp. 583–606, 1974.

[25] Y. Yao, D. Liu, Y. Che, D. Tang, S. Tang, and W. Huang, "Petrophysical characterization of coals by low-field nuclear magnetic resonance (NMR)," *Fuel*, vol. 89, no. 7, pp. 1371–1380, 2010.

[26] J. Liu, L. Xie, D. Elsworth, and Q. Gan, "CO_2/CH_4 competitive adsorption in shale: implications for enhancement in gas production and reduction in carbon emissions," *Environmental Science & Technology*, vol. 53, no. 15, pp. 9328–9336, 2019.

[27] D. O. Seevers, "A nuclear magnetic method for determining the permeability of sandstones," in *Proceedings of the SPWLA 7th Annual Logging Symposium*, pp. 1–14, Tulsa, Oklahoma, May 1966.

[28] R. L. Kleinberg and H. J. Vinegar, "NMR properties of reservoir fluids," *Society of Petrophysicists and Well-Log Analysts*, vol. 37, no. 6, pp. 20–32, 1996.

[29] C. Straley, D. Rossini, H. Vinegar, P. Tutunjian, and C. Morriss, "Core analysis by low field NMR," *Society of Petrophysicists and Well-Log Analysts*, vol. 38, no. 2, pp. 84–94, 1997.

[30] Y.-D. He, Z.-Q. Mao, L.-Z. Xiao, and Y.-Z. Zhang, "A new method to obtain capillary pressure curve using NMR T_2 distribution," *Journal of Jilin University (Earth Science Editon)*, vol. 35, no. 2, pp. 177–181, 2005.

[31] G. R. Coates, L.-Z. Xiao, and M. G. Primmer, *NMR Logging: Principles and Applications*, Gulf Publishing Company, Houston, TX, USA, 1999.

[32] S. Wang, "Analysis of rock pore structural characteristic by nuclear magnetic resonance," *Xinjiang Petroleum Geology*, vol. 30, no. 6, pp. 768–770, 2009.

[33] C. H. Sondergeld, R. J. Ambrose, C. S. Rai, and J. Moncrieff, "Micro-structure studies of gas shales," in *Proceedings of the Unconventional Gas Conference and Exhibition*, pp. 1–17, Pittsburgh, PA, USA, June 2012.

[34] A. Li, W. Ding, R. Wang et al., "Petrophysical characterization of shale reservoir based on nuclear magnetic resonance (NMR) experiment: a case study of lower Cambrian Qiongzhusi formation in eastern Yunnan Province, South China," *Journal of Natural Gas Science and Engineering*, vol. 37, pp. 29–38, 2017.

[35] C. Fangwen, D. Xue, L. Shuangfang, and J. Yiwen, "The pore characterization of the lower silurian longmaxi shale in the southeast Chongqing, China using FE-SEM, LTNA and MIP methods," *Journal of Nanoscience and Nanotechnology*, vol. 17, no. 9, pp. 6482–6488, 2017.

[36] A. Seiphoori, A. Whittle, K. Krakowiak, and H. Einstein, "Insights into diagenesis and pore structure of opalinus shale through comparative studies of natural and reconstituted materials," *Clays and Clay Minerals*, vol. 65, no. 2, pp. 135–153, 2017.

[37] J. Liu, Y.-B. Yao, D. Elsworth, D.-M. Liu, Y.-D. Cai, and L. Dong, "Vertical heterogeneity of the shale reservoir in the lower Silurian Longmaxi formation: analogy between the southeastern and northeastern Sichuan basin, SW China," *Minerals*, vol. 7, Article ID 7080151, 2017.

[38] J. Liu, Y. Yao, D. Liu, Y. Cai, and J. Cai, "Comparison of pore fractal characteristics between marine and continental shales," *Fractals*, vol. 26, no. 2, Article ID 1840016, 2018.

[39] K. S. W. Sing, "Reporting physisorption data for gas/solid systems with special reference to the determination of surface area and porosity," *Pure and Applied Chemistry*, vol. 57, pp. 603–619, 1985.

[40] H. Gao and H. Li, "Determination of movable fluid percentage and movable fluid porosity in ultra-low permeability sandstone using nuclear magnetic resonance (NMR) technique," *Journal of Petroleum Science and Engineering*, vol. 133, pp. 258–267, 2015.

[41] Y.-B. Yao and D.-M. Liu, "Petrophysics and fluid properties characterizations of coalbed methane reservoir by using NMR relaxation time analysis," *Coal Science & Technology*, vol. 44, no. 6, pp. 14–22, 2016.

[42] W. Yan, J. Sun, Y. Sun, and N. Golsanami, "A robust NMR method to measure porosity of low porosity rocks," *Microporous and Mesoporous Materials*, vol. 269, pp. 113–117, 2018.

[43] J. Li, S. Lu, J. Cai, P. Zhang, H. Xue, and X. Zhao, "Adsorbed and free oil in lacustrine nanoporous shale: a theoretical model and a case study," *Energy & Fuels*, vol. 32, no. 12, pp. 12247–12258, 2018.